Satellite Products and Services Review Board

Algorithm Theoretical Basis Document For NOAA NDE VIIRS I-band (375m) Active Fire

Compiled by the
SPSRB Common Standards Working Group

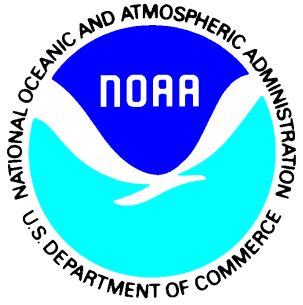

Version 1.0

June, 2020

TITLE: VIIRS ACTIVE FIRE ALGORITHM THEORETICAL BASIS DOCUMENT

AUTHORS:

Wilfrid Schroeder (NOAA/NESDIS Office of Satellite and Product Operations)

Louis Giglio (University of Maryland)

Ivan Csiszar (NOAA/NESDIS Center for Satellite Applications and Research)

Marina Tsidulko (I.M. Systems Group, Inc.)

Remarks: This document shares algorithm descriptive material with the corresponding NASA-sponsored VIIRS I-band Active Fire algorithm theoretical basis document. However, slight differences in algorithmic details exist due to differences between the NASA VIIRS Level 1B and NOAA VIIRS SDR data products that are input to the VIIRS Active Fire algorithm. This document describes the algorithm as applicable to the NOAA VIIRS SDR input data only.

DOCUMENT HISTORY
DOCUMENT REVISION LOG

The Document Revision Log identifies the series of revisions to this document since the baseline release. Please refer to the above page for version number information.

DOCUMENT TITLE: Algorithm Theoretical Basis Document Template			
DOCUMENT CHANGE HISTORY			
Revision No.	**Date**	**Revision Originator Project Group**	**CCR Approval # and Date**
1.0	5/06/2020	STAR Active Fire team	

LIST OF CHANGES

Significant alterations made to this document are annotated in the List of Changes table.

DOCUMENT TITLE: Algorithm Theoretical Basis Document Template					
LIST OF CHANGE-AFFECTED PAGES/SECTIONS/APPENDICES					
Version Number	**Date**	**Changed By**	**Page**	**Section**	**Description of Change(s)**

TABLE OF CONTENTS

LIST OF TABLES AND FIGURES

1. INTRODUCTION

This document presents the scientific background, design and anticipated performance of the 375 m I-band Active Fire (AF) algorithm for the Joint Polar Satellite System (JPSS). The AF algorithm produces two main outputs from the Visible Infrared Imaging Radiometer Suite (VIIRS) multi-spectral data, namely: (i) an image classification product (fire mask) including thematic classes such as fire/no-fire, clouds, water and clear-land pixels; and (ii) sub-pixel characterization of the instantaneous power emitted by detected fires (fire radiative power [FRP] retrievals).

The VIIRS AF algorithm described here fulfills the requirements identified in the JPSS Active Fire Environmental Data Record (EDR) specification (JPSS L1RDS.5.5.1), while addressing other user-driven requirements meant to facilitate product usage and assimilation onto ongoing fire research and applications (e.g., science data formats and nomenclature). Furthermore, those requirements provide continuity to the 750 m VIIRS M-band, the Moderate Resolution Imaging Spectroradiometer (MODIS) and the Advanced Very High Resolution Radiometer (AVHRR) active fire data records. This product consists of a hybrid algorithm combining qualities of the 375 m and 750 m VIIRS data. The higher resolution data (channels I1-I5) are the primary drivers of the fire detection component, whereas the 750 m data (specifically the dual-gain M13 channel) are used primarily in the fire radiative power (FRP) retrievals. The 375 m fire algorithm supersedes the baseline VIIRS 750 m active fire detection and characterization algorithm which was designed based on the 1 km MODIS *Fire and Thermal Anomalies* (MOD14/MYD14) Collection 6 product and incorporates code updates and methodological advances derived from several years of algorithm development and validation [Giglio et al., 2016]. Compared to other coarser resolution (≥1 km) satellite fire detection products, the VIIRS 375 m data provide greater response over fires of relatively small area, as well as improved mapping of large fire perimeters.

1.1. Product Overview

1.1.1. Product Description

The 375 m VIIRS AF product is a Level 2 data set retaining the original swath projection and geo-location information of the Level 1 input data used. A single file (or granule) comprises an orbit segment spanning multiple scans, with each individual cross-track scan describing 32 rows of pixels (Y axis), one row for each detector. Each scan row contains a total of 6400 samples (X axis) consisting of 375 m nominal resolution pixels. The number of scans stored in a single file may vary depending on the characteristics of the data processing system, whereas multiples of 48 are used. As a result, the minimum array size

of the fire mask included in the VIIRS AF product will have n=1×48 scans, or 6400×1536 elements corresponding to an ≈86 second orbit segment. The NESDIS Data Exploitation (NDE) system operating the AF algorithm at NOAA/NESDIS, by default, processes each ≈86 second granule separately. The VIIRS AF algorithm is applied to every pixel in the input day and nighttime data files, extending the detection of fires over ocean waters to allow mapping of offshore gas flaring in response to users' requests. Coastlines and inland water bodies are normally skipped during processing in order to avoid potential false alarms. Those areas are identified and masked using ancillary land/water classification data (see Section 2.2).

The image classification product (fire mask) is the primary science data set consisting of a two dimensional array with same size as the input VIIRS 375 m data used by the fire algorithm. The VIIRS AF fire mask contains nine different pixel classes; three of those classes are used to flag fire-affected pixels along with their detection confidence (see Table 2-2). FRP retrievals and other supporting data such as fire pixel image element [x] and [y], and latitude/longitude are stored in vector format, each containing *N* records describing the number of fire pixels detected (See Section 2.4).

1.1.2. Product Requirements

The requirements for the VIIRS active fire product are described in the JPSS Level 1 Requirements Supplement. (The current version is available at http://www.jpss.noaa.gov/technical_documents.html .)

1.2. Satellite Instrument Description

The AF algorithm uses data from the VIIRS instrument on the Suomi National Polar-orbiting Partnership (S-NPP) and NOAA-20 platforms and on future satellites of the Joint Polar Satellite System (JPSS). S-NPP and NOAA-20 were launched on October 28, 2011 and November 8, 2017, respectively. They are in sun synchronous orbits with a 1:30pm ascending-node orbit at an altitude of ≈829 km, separated by 50 minutes (i.e. half of an Earth orbit). It is anticipated that the algorithm described here will also be applicable to future satellites of the JPSS series without any significant alteration, assuming similar sensor performance for the input spectral bands.

The VIIRS instrument is a whiskbroom scanning radiometer with a swath width of 3060 km, providing full daily coverage both in the day and night side of the Earth. It has 22 spectral

bands covering the spectrum between 0.412 μm and 12.01 μm, including 16 moderate resolution bands (M-bands) with a spatial resolution of 750 m at nadir, 5 imaging resolution bands (I-bands) – with a spatial resolution of 375 m at nadir, and one panchromatic DNB with a 750 m spatial resolution throughout the scan. Further details can be found in the VIIRS Sensor Data Record (SDR) User's Guide (NOAA Technical Report NESDIS 142A).

2. ALGORITHM DESCRIPTION

The AF algorithm provides active fire detection and characterization information for each VIIRS granule, resulting in daily global coverage for daytime and nighttime observations. Different sets of detection criteria are used during day and night observations; night pixels are defined as those having a solar zenith angle greater than 85^{o}. The detection criteria are based on multi-spectral tests using primarily the mid-infrared (3.55-3.93 μm) channel I4 and thermal-infrared 10.5-12.4 μm channel I5 brightness temperatures of the candidate fire pixel, and the brightness temperature difference between that pixel and its background (neighboring pixels). Those primary detection tests are complemented by other multi-spectral tests in order to screen for other radiometrically bright pixels (e.g., clouds and sandy soil) that can lead to false alarms. The algorithm uses a hybrid approach to detect fires based on fixed thresholds and dynamically adjusted contextual tests. The latter utilize sampling windows of variable sizes to assess the areas surrounding candidate fire pixels. The use of adaptive detection tests allows for improved algorithm response to sub-pixel fire activity across a wide range of observation conditions. The higher resolution VIIRS 375 m data provide the basis for the detection of active fires and other thermal anomalies, whereas the 750 m data are used in the calculation of FRP as well as to discriminate potential false alarms associated with noise in the input fire- sensitive 375 m mid-infrared (I4) channel data.

2.1. Processing Outline

The VIIRS AF is a self-contained algorithm with no dependencies on other Level 2 products. It reads input SDR from VIIRS channels, plus the companion terrain-corrected geolocation file and the land/water mask (see Section 2.2). The latter is derived from MODIS based 15'' (~500m) resolution global land-water mask, which is converted into swath granules to match the input SDR file format. The input (read) module feeds 48 full scans at a time to the fire detection module. FRPs are calculated for all fire pixels detected.

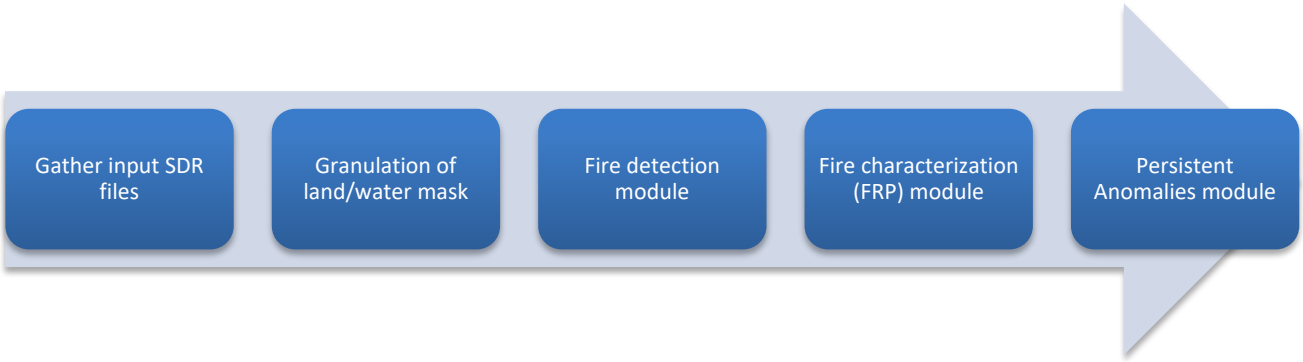

Figure 2-1: VIIRS AF algorithm processing flow. Input data are gathered (SDR) and pre-processed (granulation of land/water mask), and ingested into the fire detection module. Finally FRP is calculated for each fire pixel detected. In post-processing, potential false alarms due to persistent anomalies of industrial or nature sources are flagged.

2.2. Algorithm Input

The VIIRS 375 m fire product uses input data from all five 375 m channels (I1-I5) and the dual-gain 750 m mid-infrared data (channel M13), in addition to their corresponding quality flags (QF1) (Table 2-1). All radiance, reflectance, and brightness temperature data correspond to the calibrated top-of-atmosphere (at-sensor) values. The complementary SDR quality flag (QF1) information is used to help identify pixels showing non-nominal data quality as a result of poor calibration, pixel saturation and other data artifacts. The QF1 data are used judiciously in order to identify and avoid SDR data artifacts, thereby preventing spurious detections in the resulting AF product. A single ancillary data set is derived from gridded MODIS based global land-water mask of 15'' (~500m) resolution. A granulation process is implemented to that data set in order to create data arrays of identical dimensions and projection type as the input SDR files.

Table 2-1: List of VIIRS channels used as input to the 375 m active fire detection algorithm. The corresponding VIIRS SDR data quality flags, terrain-corrected geolocation and quarterly land- water mask data complement the list of input files used.

Channel	Spatial Resolution (m)	Spectral resolution (µm)	Primary Use
I1	375	0.60 – 0.68	Cloud & water classification
I2	375	0.846 – 0.885	Cloud & water classification
I3	375	1.58 – 1.64	Water classification
I4	375	3.55 – 3.93	Fire detection
I5	375	10.5 – 12.4	Fire detection & cloud classification
M13*	750	3.973 – 4.128	FRP retrieval, fire detection over water and across the South Atlantic magnetic anomaly region

* Aggregated (750×750 m nominal) & un-aggregated (250×750 m nominal) data are used

2.3. Theoretical Description

2.3.1. Physical Description

Actively burning fires often show a wide range of temperatures spanning several hundred Kelvins in association with flaming and smoldering phases of combustion. Typically, cooler smoldering fires show temperatures between 450 and 850 K, whereas higher temperatures ranging from 800 K to upwards of 1200 K prevail during the more intense flaming phase [Lobert and Warnatz, 1993]. Fuel type and moisture, and ambient conditions (air temperature, wind, and relative humidity) are key factors regulating biomass combustion. When medium spatial resolution sensors are considered, mid-infrared (4 μm) spectral channels are the most responsive to actively burning fires capturing most of the radiometric signal from smoldering and flaming phases of combustion during both day and nighttime parts of the orbit. The peak in emitted fire radiant energy in channel I4 makes that channel (and similarly channel M13) responsive to small sub-pixel fires occurring over a cool (≤ 300 K) background. Consequently, intense active fires (>1000 K) occupying fractional pixel areas as small as 10^{-4} may be detected. In addition to facilitating the detection of sub-pixel active fires, the rate of radiative energy released by fires observed in the 4 μm region is found to be directly related to the biomass consumed per unit time [Kaufman *et al*., 1998; Wooster *et al*., 2003].

The VIIRS active fire detection algorithms build on the NASA EOS/MODIS fire product heritage using a multi-spectral contextual algorithm to identify sub-pixel fire activity and other thermal anomalies in the Level 1 (swath) input data [Kaufman *et al*., 1998]. The baseline VIIRS 750 m active fire detection product was originally designed mirroring the MODIS Collection 4 *Fire and Thermal Anomalies* algorithm (MOD14/MYD14), although lacking key output science data layers such as the 2D fire mask and FRP retrievals [Csiszar *et al*., 2014; Giglio *et al*., 2003]. That algorithm was later replaced with the MODIS Collection 6 algorithm equivalent including all output science data layers [Giglio *et al*., 2016].

The algorithm described in this document constituted a repurposing of the VIIRS 375 m (I) channels, as none of those were originally designed for active fire detection. Most importantly, abnormal radiometric conditions involving different pixel saturation scenarios are frequently observed in the primary mid-infrared channel I4 thereby requiring special handling of the data. Building on the MOD14/MYD14 algorithm, several modifications were implemented in order to accommodate the unique characteristics associated with the VIIRS 375 m data. Detailed algorithm description is provided in the following sections. The information contained in this document is complemented by the original peer-reviewed

publication describing the initial implementation of the VIIRS 375 m global algorithm [Schroeder *et al*., 2014].

2.3.2. Mathematical Description

The VIIRS fire algorithm uses a combination of fixed and contextual tests to detect active fires and other thermal anomalies in both daytime and nighttime (solar zenith angle $\geq 90^{o}$) parts of the orbit. The detection criteria are based on multi-spectral tests using primarily the mid-infrared (channel I4) and long wave- infrared (channel I5) data, complemented by cloud and water classification schemes as described below.

2.3.2.1 *Cloud and Water Pixel Classification*

The cloud classification scheme builds on the MODIS fire product [Giglio *et al*., 2003; 2016] and is designed to mask optically thick clouds. The resulting cloud mask is made intentionally liberal in order to minimize fire detection omission errors under translucent clouds (e.g., cirrus) and in partially covered pixels. Cloud-covered pixels are identified in the daytime data using the following criteria:

$$BT_5 < 265 \text{ K} \text{ OR}$$
$$\rho_1+\rho_2 > 0.9 \text{ AND } BT_5 < 295 \text{ K} \text{ OR}$$
$$\rho_1+\rho_2 > 0.7 \text{ AND } BT_5 < 285 \text{ K}$$

where ρ_i and BT_i are the top-of-atmosphere reflectance and brightness temperature in VIIRS 375 m channel *i,* respectively. Nighttime cloud pixels are identified using:

$$BT_5 < 265 \text{ K AND } BT_4 < 295 \text{ K}$$

Pixels identified as clouds skip any subsequent fire detection processing and are also excluded from background characterization. Complementing the cloud masking, water pixels are classified using:

$$\rho_1 > \rho_2 > \rho_3$$

The test above can successfully identify most water bodies in the daytime data although it tends to omit sediment-filled water pixels along shorelines, and cause commission errors over burn scars. Those limitations have no observable impact on the overall fire pixel detection and characterization performance. The internal water mask complements the available VIIRS land-water mask which builds on the MODIS 250 m water classification product [Carroll *et al*., 2009]. All water pixels undergo subsequent processing to allow detection of gas flares and other thermal anomalies.

2.3.2.2 *Fixed Threshold Tests*

Fire pixels are first identified in the day and nighttime data using a combination of fixed threshold tests based on the observation scenario. Fire pixels detected using these tests show a stronger radiometric signature in either channel I4 or I5 data, and tend to be unequivocally associated with active fires or high intensity thermal anomalies. Fire pixels detected using these tests are initially assigned "*medium confidence*" or "*high confidence*" classes as listed below.

In case of unsaturated nighttime data, the following test is used:

$BT_4 > 320$ K AND $QF_4 = 0$ $(nighttime\ only)$

Where QF_4 is the VIIRS channel I4 quality flag value. *("Medium confidence")*

Saturated daytime and nighttime fire pixels are identified using the following criteria:

$BT_4 = 367$ K AND $QF_4 = 9$ AND $QF_5 = 0$ $(daytime\ or\ nighttime)$ AND
$BT_5 > 290$ K AND $\rho_1 + \rho_2 < 0.7$ $(daytime\ only)$

Where QF_5 is the VIIRS channel I5 quality flag value. *("High confidence")*

Finally, cases involving folding of channel I4 data are identified using:

$\Delta BT_{45} < 0$ AND $BT_5 > 325$ K AND $QF_5 = 0$ $(daytime\ only)$ OR
$\Delta BT_{45} < 0$ AND $BT_5 > 310$ K AND $QF_5 = 0$ $(nighttime\ only)$ OR
$BT_4 = 208$ K AND $BT_5 > 335$ K $(nighttime\ only)$

Where ΔBT_{45} is the brightness temperature difference between channels I4 and I5. *("High confidence")*

2.3.2.3 *Potential Background Fires*

Potential background fire pixels can affect the detection and characterization of individual fire pixels and therefore must be identified and masked out accordingly. The following tests are used to identify those pixels:

$BT_4 > 335\ K$ AND $\Delta BT_{45} > 30$ K $(daytime\ only)$ OR
$BT_4 > 300\ K$ AND $\Delta BT_{45} > 10$ K $(nighttime\ only)$

In addition to the tests above, pixels associated with folding of channel I4 data (typically characterized by artificially low BT_4) are also considered background pixels.

2.3.2.4 *Avoiding Bright Reflective Targets*

Solar reflection over bright surfaces (e.g., sand banks along riverbeds) can induce high brightness temperatures on channel I4 daytime data, causing potential confusion with active fires. Those areas are identified and avoided using the following criteria:

$$\rho_3 > 0.3 \text{ AND } \rho_3 > \rho_2 \text{ AND } \rho_2 > 0.25 \text{ AND } BT_4 \leq 335 \text{ K}$$

Sun glint is a form of recurring observation phenomenon also known to lead to false alarms in satellite fire detection products. Examples of false alarm-prone areas associated with solar reflection include large metallic rooftops in industrial parks, small/undetected water bodies, and other bright surfaces in urban areas. In order to reduce the frequency of those occurrences, pixels identified with the following tests are assigned a '*sun glint*' class and not considered for candidate fire pixel selection (Section 2.3.2.5):

$$cos\theta_g = cos\theta_v \times cos\theta_s - sin\theta_v \times sin\theta_s \times cos\phi$$

$$\theta_g < 15^o \text{ AND } \rho_1 + \rho_2 > 0.35$$
$$\text{OR}$$
$$\theta_g < 25^o \text{ AND } \rho_1 + \rho_2 > 0.4$$

Where θ_v and θ_s are the view and solar zenith angles, respectively, and ϕ is the relative azimuth angle. Note that additional sun glint may occur from non-horizontal surfaces such as solar farms. Such cases are flagged using the persistent anomaly flag described in Section 2.3.3.

2.3.2.5 *Candidate Fire Pixels*

Candidate fire pixels are selected using relatively liberal tests in order to include all potential pixels showing thermal anomalies on channel I4 according to:

$$BT_4 > BT_{4S} \text{ AND } \Delta BT_{45} > 25 \text{ K} \quad (daytime\ only) \text{ OR}$$
$$BT_4 > 295 \text{ K AND } \Delta BT_{45} > 10 \text{ K} \quad (nighttime\ only)$$

Where BT_{4S} is a dynamically-adjusted background value calculated using channel I4 brightness temperature data based on a 501×501 sampling window centered on the candidate fire pixel. This initial large-area sampling accommodates variations in

background conditions, adding flexibility to candidate fire pixel selection. It is intended to improve algorithm sensitivity to fires occurring in colder high latitude regions, while reducing false alarm rates in lower latitudes consisting of warmer background. The large area background sampling excludes all pixels previously classified as cloud, water bodies, and potential background fire pixels, as well as any pixel with non-zero quality flag including fill values associated with *bowtie* deletion samples [Wolfe *et al*., 2013]. BT_{4S} is defined as:

$$BT_{4M} = MAX[325, M+25] \text{ K}$$
$$BT_{4S} = MIN[330, BT_{4M}] \text{ K}$$

Where *M* is the BT_4 median value calculated for the 501×501 window. The sampling window must contain a minimum of 10 valid observations otherwise BT_{4S} is set to 330 K. Furthermore, BT_{4S} is only derived for daytime data allowing the candidate fire pixel brightness temperature on channel I4 to vary between a minimum of 325 K to a maximum of 330 K in order to accommodate scene-dependent changes in background conditions. Nighttime background conditions are found to be less variable, therefore the algorithm uses a single fixed value to define candidate fire pixels at night. For daytime, pixel is flagged as candidate using single fixed value as well, even if it did not pass the 501x501 window test described above. The result of this test is flagged separately (see bits 10&11 in Table 2-3).

2.3.2.6 *Contextual Fire Detection Tests*

The contextual tests use a dynamic sampling window to characterize the background conditions around each individual candidate fire pixel. The sampling window is allowed to vary from a minimum of 21×21 elements centered on the candidate pixel, to a maximum of 61×61 (daytime) or 71x71 (nighttime) elements until ≥25% or ≥10 valid pixels are encountered. Valid pixels exclude clouds, background fire pixels, non-nominal quality data, and are limited to same-class pixels (i.e., candidate fire pixels over land (water) use land (water) background pixels only). Candidate fire pixels lacking proper background characterization are assigned the "*unclassified*" class. Daytime candidate fire pixels having ≥4 background fire pixels in the sampling window, or having background fire pixels in excess of 10% of the valid background pixels must go through the following test:

$$\rho_2 > 0.15 \text{ AND } BT'_{4B} < 345 \text{ K AND } \delta'_{4B} < 3 \text{ K } AND\ BT_4 < BT'_{4B} + 6 \times \delta'_{4B}$$

Where BT'_{4B} and δ'_{4B} are the mean brightness temperature and mean absolute deviation, respectively, calculated using the potential background fire pixels. Candidate fire pixels that satisfy the criteria above are excluded from further processing and assigned a fire-free (water or land) pixel class. The tests below describe the subsequent daytime and nighttime data processing criteria applied to the remaining candidate fire pixels:

$Daytime$:

$\Delta BT_{45} > \Delta BT_{45B} + 2 \times \delta_{45B}$
AND
$\Delta BT_{45} > \Delta BT_{45B} + 10\ \mathrm{K}$
AND
$BT_4 > BT_{4B} + 3.5 \times \delta_{4B}$
AND
$BT_5 > BT_{5B} + \delta_{5B} - 4\ \mathrm{K}\ \mathrm{OR}\ \delta'_{4B} > 5\ \mathrm{K}$

$Nighttime$:
$\Delta BT_{45} > \Delta BT_{45B} + 3 \times \delta_{45B}$
AND
$\Delta BT_{45} > \Delta BT_{45B} + 9\ \mathrm{K}$
AND
$BT_4 > BT_{4B} + 3 \times \delta_{4B}$

Where ΔBT_{45B} and BT_{iB} denote the mean channel I4-I5 brightness temperature difference and the mean brightness temperature on channel i, respectively, calculated using the valid background pixels; δ_{45B} and δ_{4B} are the mean absolute deviation calculated for channel I4-I5 brightness temperature difference and channel I4, respectively, also using the valid background pixel data. Candidate fire pixels meeting the criteria above are assigned a '*nominal'* confidence fire pixel class.

2.3.2.7 *Secondary Tests*

Two additional tests are applied to the data in order to (i) identify residual fire pixels not detected with the criteria above, and (ii) mark down potential low confidence fire pixels. The first test targets less common pixel saturation and folding scenarios using the following criteria:

$BT_5 \geq 325\ \mathrm{K}\ \mathrm{OR}\ BT_4 = 367\ \mathrm{K}\ \mathrm{OR}\ \Delta BT_{45} < 0\ \mathrm{K}$

Pixels that meet such criteria and have one or more adjacent fire pixels of '*nominal*' or '*high*' confidence (among the eight immediate neighbors) are assigned a '*low'* confidence fire class. The second test targets residual false alarms occurring along Sun glint areas.

The following test is applied to all '*nominal confidence*' fire pixels:

$\Delta BT_{45} \leq 30\ \mathrm{K}\ \mathrm{OR}\ \theta_g < 15^{\mathrm{o}}$

Pixels meeting the above criteria will be assigned a '*low confidence*' fire pixel class if one of the following conditions apply:

(i) two or more adjacent '*Sun glint*' pixels are found
(ii) no adjacent '*high confidence*' pixels are found and BT_4 is less than 15 K higher than adjacent pixels

2.3.2.8 *Nighttime South Atlantic Magnetic Anomaly Filter*

Noise associated with the South Atlantic magnetic anomaly is particularly pronounced in the mid-infrared channel I4 data driving the detection of fires and thermal anomalies. The noise condition is found predominantly at night, with only few and sparse occurrences during the day. Given the random nature and radiometric signal characteristics of the resulting channel I4 noise, which often mimic those of actual fires, several spurious fire pixels are normally produced over the affected region (Figure 2-2). Data artifacts are often linked to single, stand-alone pixels showing abnormally high brightness temperature on channel I4. In order to address the problem, the algorithm uses co-located un-aggregated M13 brightness temperature data to independently verify nighttime fire pixels. Despite their similar spectral characteristics, channel M13 shows significantly lower rates of data contamination compared to channel I4. In addition to that, channel I4 and M13 occurrences are found to be predominantly independent from each other.

The filter first creates a modified aggregated M13 data array by replacing the mean value aggregation scheme with a maximum value method. This approach minimizes fire signal loss as a result of the normal aggregation scheme. The suspicious 375 m fire pixel is subsequently co-located to the modified M13 data array, after which the coincident M13 aggregated pixel is selected for further analysis. In order to be confirmed as a '*nominal*' or '*high*' confidence fire pixel, the coincident M13 pixel brightness temperature must be ≥ 2 K than all of the adjacent M13 pixels. Pixels that failed that test are downgraded to a fire-free ('*water*' or '*land*') class and marked with a unique quality flag (see Table 2-3).

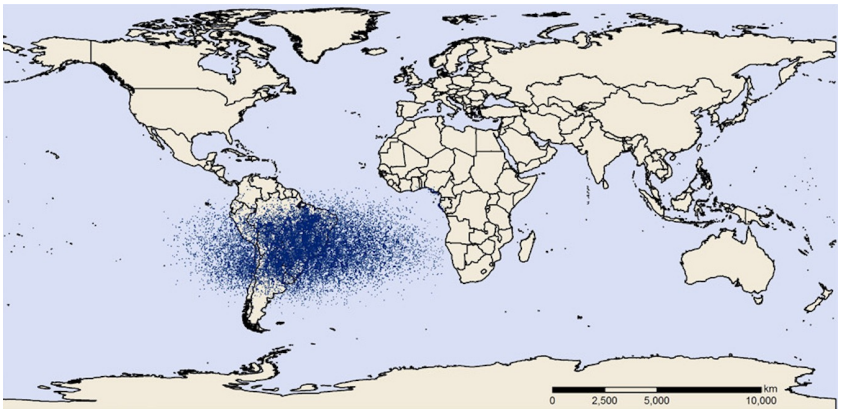

Figure 2-2: Spurious VIIRS 375 m fire detections associated with the South Atlantic

magnetic anomaly during 01-30 August 2013 (adapted from Schroeder *et al*. [2014]).

2.3.2.9 *Persistence Test*

Some residual noise in the input data may propagate through the algorithm leading to few and isolated spurious detections most easily found over ocean waters. Such cases are typically associated with random sensor noise or with infrequent manifestation of South Atlantic magnetic anomaly on daytime data. In order to improve handling of those cases, the algorithm includes a persistence test applied to fire pixels detected over water. Based on that test, '*low*', '*nominal*' and '*high*' confidence fire pixels detected over water must show distinguishable heat signature on channel M13. The test uses the same approach and modified M13 aggregated data array described in Section 2.3.2.8, requiring a slightly higher brightness temperature difference of 2.5 K between the target M13 pixel and the adjacent ones. Pixels failing that initial test must show temporal persistence consisting of a minimum of 3 co-located detections in the previous 30 days in order to be confirmed. Pixels lacking M13 channel heat signature or persistence indication are downgraded to fire-free ('*water*' or '*land*') pixels and marked up with unique quality flags (bits 19-21 on Table 2-3).

2.3.2.10 *Fire Radiative Power Retrieval*

Because of the frequent fire pixel saturation in the mid-infrared I4 channel, fire radiative power retrievals are calculated using co-located M13 channel data. The approach utilizes 375 m data to identify fire pixels and to assist in the selection of valid background pixels. Co-located M13 aggregated radiances coinciding with the fire-affected and background pixels are used in the FRP retrieval following Wooster *et al*. [2003], which is represented by (assuming unit atmospheric transmittance and surface emissivity):

$$FRP = \frac{A\sigma(L_{13} - L_{13B})}{a} \cdot 10^{-6}$$

Where A is the pixel area which varies as a function of scan angle, σ is the Stefan-Boltzmann constant (5.67×10^{-8} $Wm^{-2}K^{-4}$),
a is a channel-specific constant (VIIRS M13 = 2.88×10^{-9} $Wm^{-2}sr^{-1}\mu m^{-1}K^{-4}$), and
L_{13} and L_{13B} are the M13 channel fire pixel and mean background radiances, respectively.

Despite being extremely rare, M13 pixel saturation may occur over very large and intense active fires. Normally, that condition will trigger the appropriate quality flag for the affected pixel in the input data, which may carry a fill (non-usable) radiance value. In that event, the fire pixel may still be detected (granted that the algorithm is able to resolve it using the available data) whereas the FRP retrieval will be set to zero. Other situations involving challenging FRP retrieval (e.g., insufficient background data) may also result in fire pixels

accompanied by null FRP values. We note that such cases are rather infrequent. A single pixel 750 m FRP retrieval is divided among the number of coincident 375 m fire pixels, with each sub-pixel receiving the same resulting value in MW (Figure 2-3).

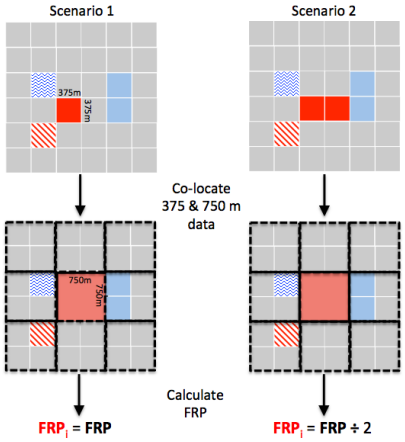

Figure 2-3 FRP calculation using a combination of VIIRS 375 m and 750 m data. The former is used to identify fire-affected (solid and dashed red), cloud (solid blue), water pixels (dashed blue), and valid background pixels (gray; in this case representing fire-free land surface). Co-located M13 channel radiance data (750 m; black dashed outline) coinciding with fire pixel (red shade) and valid background pixels (gray-only) are used in the FRP calculation. In scenario 1, the single 750 m retrieval (center pixel; **FRP**) is assigned to the single coincident 375 m fire pixel (solid red; **FRP**$_i$, where *i* is the 375 m fire-affected sub-pixel index). In scenario 2, the single 750 m FRP retrieval is split between the two coincident 375 m fire-affected sub-pixels, so that **FRP**$_i$ = **FRP**÷2.

2.3.3 Persistent anomaly flags

The operational 375 m NDE VIIRS Active Fire product also includes flags that indicate the presence of potential false fire detections due to non-biomass burning related radiative signal, such as reflection from solar farms, volcanos, gas flares. The flags are added based on colocation of fire detections with published or empirically determined persistent anomalies as follows:

0 – no persistent anomaly
1 - oil or gas flare (based on Liu et al., 2017)
2 – volcano (Global Volcanism Program, Smithsonian Institution, 2013)
3 – solar panel (empirically determined, CONUS only)
4 – urban (currently not used)
5 – unclassified (empirically determined)

2.4. Algorithm Output

The VIIRS active fire algorithm output contains 26 primary science data

sets, in addition to the algorithm's quality flag (see Table 2-3). The individual science data sets are named as follows:

'*fire mask*' = image classification array (2D)
'*FP_line*' = granule line of fire pixel
'*FP_sample*' = granule sample of fire pixel
'*FP_latitude*' = latitude of fire pixel (degrees)
'*FP_longitude*' = longitude of fire pixel (degrees)
'*FP_T4*' = channel I4 brightness temperature of fire pixel (kelvin)
'*FP_T5*' = channel I5 brightness temperature of fire pixel (kelvin)
'*FP_MeanT4*' = channel I4 mean background brightness temperature (kelvin)
'*FP_MeanT5*' = channel I5 mean background brightness temperature (kelvin)
'*FP_MeanDT*' = mean background I4-I5 brightness temperature difference (kelvin)
'*FP_MAD_T4*' = background channel I4 brightness temperature mean absolute deviation (kelvin)
'*FP_MAD_T5*' = background channel I5 brightness temperature mean absolute deviation (kelvin)
'*FP_MAD_DT*' = background I4-I5 brightness temperature difference mean absolute deviation (kelvin)
'*FP_power*' = fire radiative power (MW)
'*FP_M13*' = channel M13 radiance of fire pixel ($W.m^{-2}.sr^{-1}.\mu m^{-1}$)
'*FP_MeanM13*' = channel M13 mean background radiance ($W.m^{-2}.sr^{-1}.\mu m^{-1}$)
'*FP_AdjCloud*' = number of adjacent cloud pixels
'*FP_AdjWater*' = number of adjacent water pixels
'*FP_WinSize*' = number of adjacent water pixels
'*FP_confidence*'= detection confidence (7=low, 8=nominal, 9=high)
'*FP_day*' = day flag for fire pixel (0=night, 1=day)
'*FP_SolZenAng*'= solar zenith angle of fire pixel (degrees)
'*FP_SolAzAng*' = solar azimuth angle of fire pixel (degrees)
'*FP_ViewZenAng*'= view zenith angle of fire pixel (degrees)
'*FP_ViewAzAng*' = view azimuth angle of fire pixel (degrees)
'FP_PersistentAnomalyCategory' = persistent industrial or nature source

The '*fire mask*' consists of an 8-bit integer two-dimensional array with the same number of elements as the input SDR data array (Figure 2-4). Distinct pixel classes are used for land, water, cloud and fire pixels, plus additional classes indicating non- processed pixels and pixels with undefined classification ('*unclassified*') (Table 2-2). The latter describes those cases when background statistics cannot be retrieved preventing proper pixel classification. Fire pixel confidence classes ('*low*', '*nominal*' and '*high*') are representative of the observation conditions associated with each detection (see Section 2.3.2). The additional data sets output by the algorithm consist of individual sparse arrays containing image line, column, longitude, latitude, FRP, detection confidence, among other parameters for all fire

pixels detected.

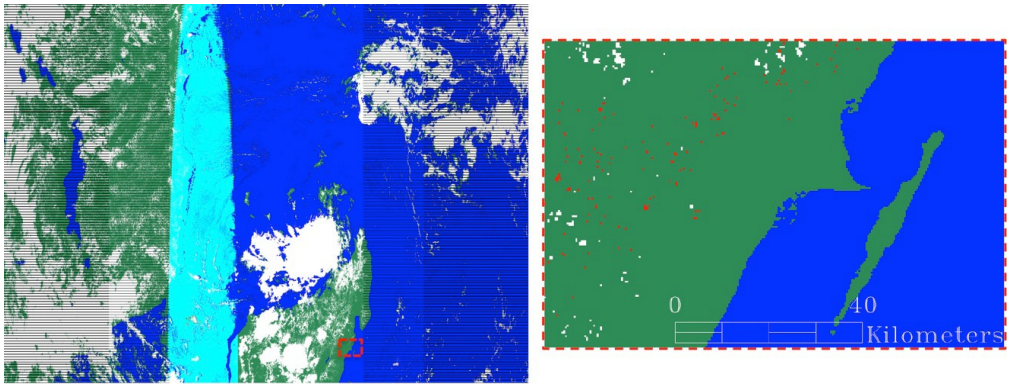

Figure 2-4: S-NPP/VIIRS 375 m active fire detection classification product (mask) derived for a granule acquired on 22 November 2015 at 1035UTC over parts of northern Madagascar and southeast Africa (left). Right panel shows magnified subset containing land (green), water (blue), clouds (white) and fire (red) pixels. Glint (cyan) and *bowtie* deletion (black) pixels are also visible in the large image.

Table 2-2: VIIRS 375 m '***fire mask***' data set classes.

Pixel Class	Definition
0	Not processed
1	*On-board Bowtie* deletion
2	Sun glint
3	Water
4	Clouds
5	Land
6	Unclassified
7	Low confidence fire pixel
8	Nominal confidence fire pixel
9	High confidence fire pixel

A two-dimensional array complements the fire mask output providing quality assurance (QA) information for every pixel processed. The QA data are stored in 32- bit unsigned integer format populated with several fields that together can be used to reconstruct some of the key observation conditions pertinent to each pixel analyzed. Bits 0-6 describe the overall (nominal/non-nominal) quality of all input files used, followed by bits 7-18 describing primary and secondary fire detection tests. Bits 19-22 are used to mark pixels associated with detection over water (persistence test) and/or *bowtie* conditions. (In order to reduce duplication, the upstream VIIRS SDR algorithm deletes from processing some pixels in overlapping area between neighboring scans; the overlapping is a result of bowtie effect of a satellite scan. VIIRS data processing applies bowtie deletion twice – first on-board for

smaller amount of pixels, and second time on-ground with expanded bowtie deletion zones. While it is impossible to process pixels in on-board deletion zones due to lack of information, pixels in on-ground deletion zones could be processed and a fire pixel could be detected. Such fire is flagged indicating that it is located in on-ground bowtie deletion zone). Bits 23-25 indicate potential false alarm due to persistent anomaly (see section 2.3.3), whereas bits 26-31 are reserved for future use.

Table 2-3: VIIRS 375 m fire detection '*algorithm QA*' data set bits and definition.

Bit	Description
0	Channel I1 quality (0 = nominal (or nighttime), 1 = non-nominal)
1	Channel I2 quality (0 = nominal (or nighttime), 1 = non-nominal)
2	Channel I3 quality (0 = nominal (or nighttime), 1 = non-nominal)
3	Channel I4 quality (0 = nominal, 1 = non-nominal)
4	Channel I5 quality (0 = nominal, 1 = non-nominal)
5	Geolocation data quality (0 = nominal, 1 = non-nominal)
6	Channel M13 quality (0 = nominal, 1 = non-nominal)
7	Unambiguous fire (0 = false, 1 = true [night only])
8	Background pixel (0 = false, 1 = true) $BT_4 > 335$ K AND $\Delta BT_{45} > 30$ K OR saturation/folding (day) $BT_4 > 300$ K AND $\Delta BT_{45} > 10$ K OR saturation/folding (night)
9	Bright pixel rejection (0 = false, 1 = true) $\rho_3 > 30\%$ AND $\rho_3 > \rho_2$ AND $\rho_2 > 25\%$ AND $BT_4 \leq 335$K
10	Candidate pixel (0 = false, 1 = true) $BT_4 > 325$ K AND $\Delta BT_{45} > 25$ K (daytime) $BT_4 > 295$ K AND $\Delta BT_{45} > 10$ K (nighttime)
11	Scene background (0 = false, 1 = true) $BT_4 >$ MIN([330, BT_{4M}]) (day)
12	Test 1 (0 = false, 1 = true) $\Delta BT_{45} > \Delta BT_{45B} + 2\times\delta_{45B}$ (day) $\Delta BT_{45} > \Delta BT_{45B} + 3\times\delta_{45B}$ (night)
13	Test 2 (0 = false, 1 = true) $\Delta BT_{45} > \Delta BT_{45B} + 10$ K (day) $\Delta BT_{45} > \Delta BT_{45B} + 9$ K (night)
14	Test 3 (0 = false, 1 = true) $BT_4 > BT_{4B} + 3.5\times\delta_{4B}$ (day) $BT_4 > BT_{4B} + 3\times\delta_{4B}$ (night)
15	Test 4 (0 = false, 1 = true) (day) $BT_5 > BT_{5B} + \delta_{5B} - 4$ K OR $\delta_{4B} > 5$ K
16	Pixel saturation condition (0 = false, 1 = true) (day) $BT_5 \geq 325$ K OR $BT_4 = 367$ K OR $\Delta BT_{45} < 0$
17	Glint condition (0 = false, 1 = true) (day) $\Delta BT_{45} \leq 30$ K OR Glint (θ_g) < 15°
18	Potential South Atlantic magnetic anomaly pixel (0 = false, 1 = true)
19	Fire pixel over water (0 = false, 1 = true)
20	Persistence test (0 = false, 1 = true) BT_{13}-MAX[BT_{13B}] < 2.5 K

21	Persistence test (0 = false, 1 = true) Number of previous co-located detections < 3
22	Residual *bowtie* pixel (0 = false, 1 = true)
23-25	Persistent anomaly category
26-31	Reserved for future use

2.5. Performance Estimates

2.5.1. Test Data Description

Prior to operations, the algorithm was rigorously tested in developmental environment. Near real time runs are performed since early 2018, both for S-NPP and NOAA-20. The outputs were thoroughly tested by comparison with current operational (750m M-band) active fire product; results of these tests are described in following sections.

For the NDE operations, a set of S-NPP and NOAA-20 test granules with different fire conditions was created and the outputs between the delivered code and the offline version were compared; all of the output parameters were found identical. Further near real time testing of the delivered code is being performed prior to sending it to the NDE system for pre-operational testing.

After the NDE unit and system tests are performed and outputs are shown to be identical to the offline version, the code is sent to Integration & Testing stream for running in a pre-operational environment on near real-time data. The output for one full day which consists of about 1000 granules is sent back to developers for verification.

2.5.2. Sensor Effects

The 375 m data describe the nominal resolution after native pixels are spatially aggregated (Figure 2-5). The aggregation scheme changes across three distinct image regions. In the first region (nadir to 31.59^{o} scan angle), three native pixels are aggregated in the along scan (cross-track) direction to form one data sample in the Level 1 image. In the second region (31.59^{o} to 44.68^{o} scan angle), two native pixels are aggregated to form one data sample. Finally in the third and last region (44.68^{o} to 56.06^{o} - edge of swath) one native pixel will result in one data sample. All five 375 m channels are aggregated onboard the spacecraft before the data are transmitted to the ground stations. The input 750 m dual-gain M13 channel data undergo a similar aggregation scheme although the data reduction is performed after the ground stations receive the native resolution data from the satellite. In order to maximize performance, the algorithm uses both aggregated and un-aggregated M13 data.

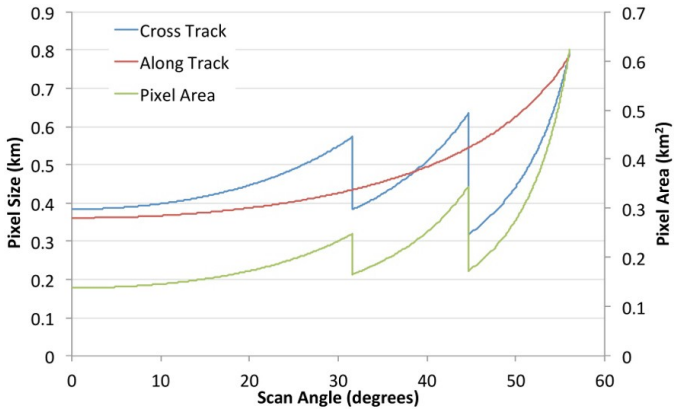

Figure 2-5: Spatial resolution of VIIRS imager data (I bands) as a function of scan angle. The three distinct regions describe data aggregation zones extending from nadir to the edge of the swath.

Given the unique spatial and spectral resolution of the data, the fire detection algorithm was customized and tuned in order to optimize its response over small fires while balancing the occurrence of false alarms. Frequent saturation of the mid- infrared I4 channel driving the detection of active fires demands additional tests and procedures in order to avoid pixel classification errors. Pixel saturation occurs most often over large and/or intense heat sources (e.g., wildfires) and is typically identified in the input data with the use of the companion quality flag. Under more extreme conditions, very large active fires (e.g., crown fires) can greatly exceed the effective saturation temperature on channel I4 leading to a complete folding of the digital number (DN) associated with the affected pixel. Application of the normal calibration parameters to those anomalous DN values results in abnormally cold brightness temperature values equal to or near the low end of that channel's dynamic range (208 K). The companion quality flags may also be used to properly identify and process those pixels. A third and more challenging scenario describing channel I4 saturation involves the mixing of saturated and unsaturated data during onboard aggregation. Such occurrences result in artificially low brightness temperatures accompanied by nominal quality flags for the affected pixels. Under those conditions, complementary channel I5 data may be used to try and identify the corrupted channel I4 pixels. Overall, the low (≈358 K) effective saturation temperature on channel I4 results in ≈9% discernable fire pixel saturation rate associated with all three scenarios above (in addition to a yet unknown percentage of more subtle and therefore indistinguishable saturation). Consequently, sub-pixel fire characterization should be avoided in that channel. That limitation is addressed in the product with the use of co-located M13 dual-gain channel data. The combination of higher (≈659 K) saturation temperature and lower spatial resolution results in extremely rare pixel saturation occurrence in the M13 data making it suitable for such application.

Another anomalous condition affecting the I4 channel involves the occurrence of spurious brightness temperature data as a result of the South Atlantic magnetic anomaly. The geographic area where the problem is most commonly found extends from 110°W <> 11°E and 7°N <> 55°S (Cabrera *et al*., 2005; Casadio *et al*., 2012). The impact of the magnetic anomaly is evidenced by artificially high brightness temperature values occurring predominantly in the nighttime I4 channel data. These occurrences are typically associated with nominal data quality and therefore cannot be readily identified using the available quality flags. On average, individual channel I4 pixels affected by the anomaly may depart from the background by 15–30 K thereby creating similar radiometric responses associated with actual nighttime fire-affected pixels at both absolute and contextual levels. No discernable impact on nighttime I5 channel data quality was found associated with the magnetic anomaly.

2.5.3. Retrieval Errors

The VIIRS active fire algorithm is a sensor-specific implementation of the heritage MODIS Thermal Anomalies / Fire algorithm. As such the performance of the algorithm can be traced back to MODIS performance, which has been documented via multiple peer-reviewed publications [e.g. Morisette et al., 2005a; Morisette et al., 2005b; Csiszar et al., 2006; Schroeder et al., 2008a; Schroeder et al., 2008b; Csiszar and Schroeder, 2008].

Additional evaluation is performed for the 375m active fire algorithm. A theoretical fire detection envelope was calculated by simulating different fire scenarios applied to actual VIIRS 375 m global imagery. Fires were simulated assuming areas ranging from 2 to 250 m^2, and temperatures ranging from 400 to 1200 K. Fire radiances were derived at 2 m^2 and 10 K intervals for both I4 and I5 channels using the instrument's spectral response functions, and assuming blackbody emission. A total of 10 daytime and 10 nighttime VIIRS L1B (SDR) granules acquired during August 2013 were randomly selected covering different geographic areas, including low and high latitude regions, with variable levels of fire activity.

For every image, 10 pixels were selected along nadir and apart from each other, and when possible, near areas of fire activity in order to best represent regional fire- prone conditions. Simulated fire radiances and actual background radiances were area-weighted to provide realistic BT_4 and BT_5 pixel values representative of actual observation conditions. The active fire detection algorithm was then applied to the data containing simulated active fire pixel surrounded by genuinely observed background pixels. Figure 2-6 shows the 50% probability of detection curves derived for the algorithm using the global daytime and nighttime data sample. Improved nighttime performance resulted from the more homogeneous background conditions, which tends to enhance the algorithm's response to

relatively small heat sources.

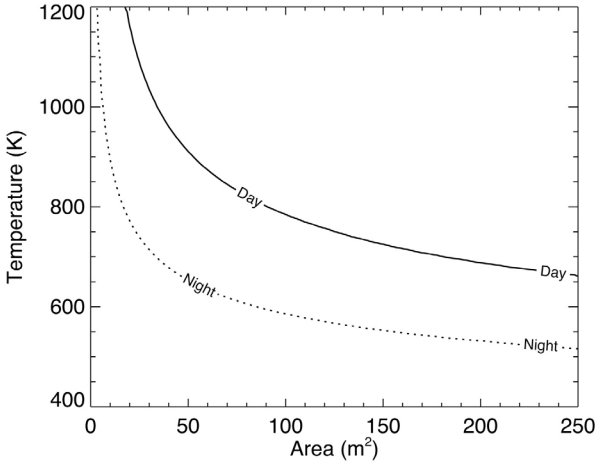

Figure 2-6: Theoretical 50% probability of fire detection curves derived for the VIIRS algorithm as a function of fire area and temperature using daytime and nighttime data (adapted from Schroeder *et al*. [2014]).

2.5.4. Numerical Computation Considerations

The Active Fire implementation employs simple tests and does not employ any numerically complex or unstable algorithms.

2.5.5. Programming and Procedural Considerations

There is one processing unit in NDE AF-Iband, it is operated by Perl driver script. The unit performs the following:

- Reads VIIRS GEO-Terrain corrected input and generates granulated land-water mask.
- Reads VIIRS SDR data (I01, I02, I03, I04, I05, M13, IVCDB) in HDF5 format.
- Extracts metadata from HDF5 files for subsequent conversion into NetCDF attributes in output NDE AF-Iband product.
- Invokes the AF algorithm which provides all necessary calculations to determine fire locations and properties.

- Outputs fire product in NetCDF format, including NDE-specific granule attributes.
- Applies post-processing for adding persistent anomaly flag to the product.

All the codes employed prior to the persistent anomalies step are written in C language; the persistent anomalies part is written in C++.

2.5.6. Quality Assessment and Diagnostics

The VIIRS AF data quality assessment is built on product inter-comparison using active fire data from both S-NPP and NOAA-20 VIIRS sensors. Inter-comparison with operational 750m active fire product was performed, with data analyzed both globally and regionally. Figure 2-7 shows detection rates relative to the I-band product as a function of the number of I-band resolution detections within the M-band pixel footprint. Frequency of M-band detections without a single I-band detection can be interpreted as a proxy for commission errors for the M-band product, but may also indicate some possible omissions by the I-band algorithm. Detection rates increase with increasing number of I-band detections. Analysis demonstrate good consistency of detection rates between Suomi NPP and NOAA-20. Significant differences between daytime and nighttime detection rates indicate a more conservative performance of the nighttime M-band algorithm.

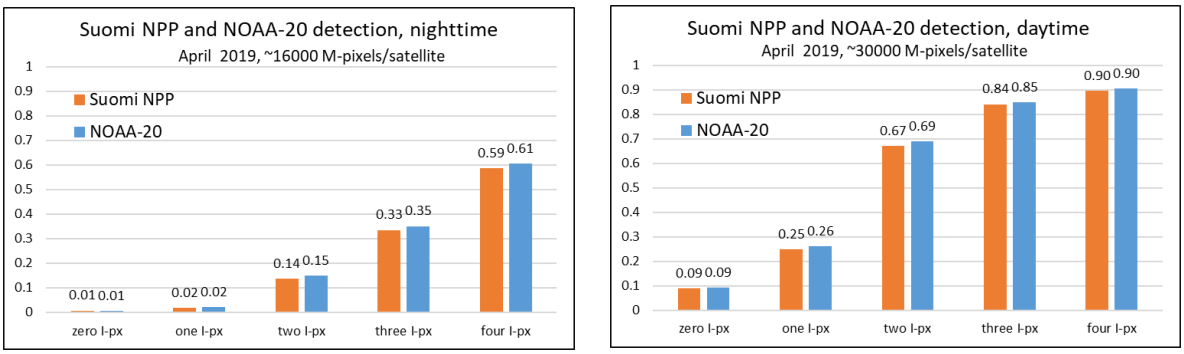

Figure 2-7: Daytime (left) and nighttime (right) relative detection performance between the operational 750m M-band and the 375m I-band VIIRS active fire products

Global analysis of fire radiative power (FRP) (Fig. 2-8) shows that I-band FRP is higher than M-band FRP which is a result of significantly more fire detections in I-band algorithm, especially at nighttime.

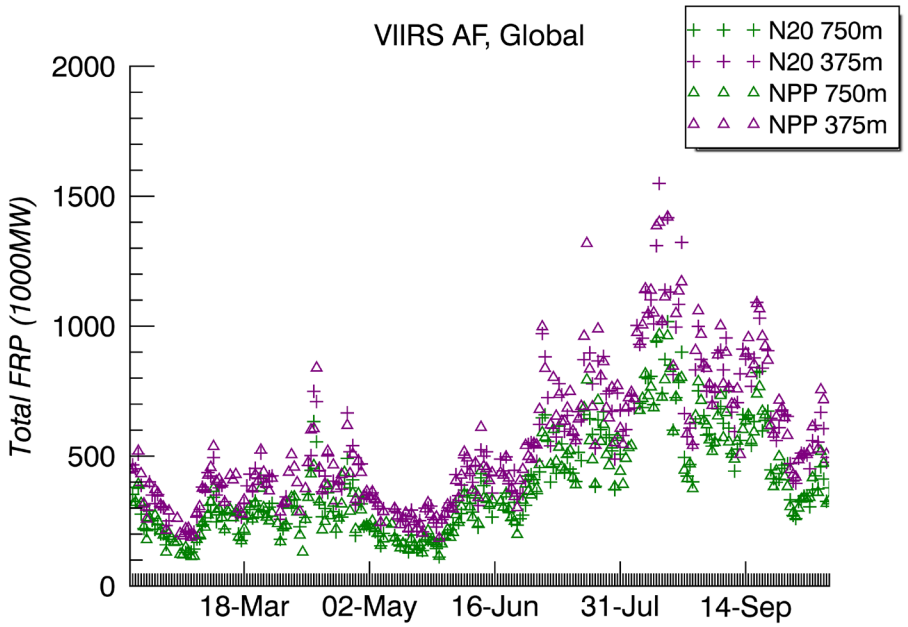

Figure 2-8: Global FRP for S-NPP and NOAA-20, 750m (M-band) and 375m (I-band) products; March-September 2018.

S-NPP and NOAA-20 orbits are 50 minutes apart which results in viewing a particular fire in different parts of satellite swath, sometimes with very different scan angles. Also, if a fire is small and short in duration it could be detected by one satellite and not detected by another. While agreement between satellites is expected it is not considered to be a perfect match. Figure 2-9 demonstrates agreement in global FRP between two satellites as expected. It also shows that the I-band algorithm can detect fires with significantly smaller FRP than the M-band.

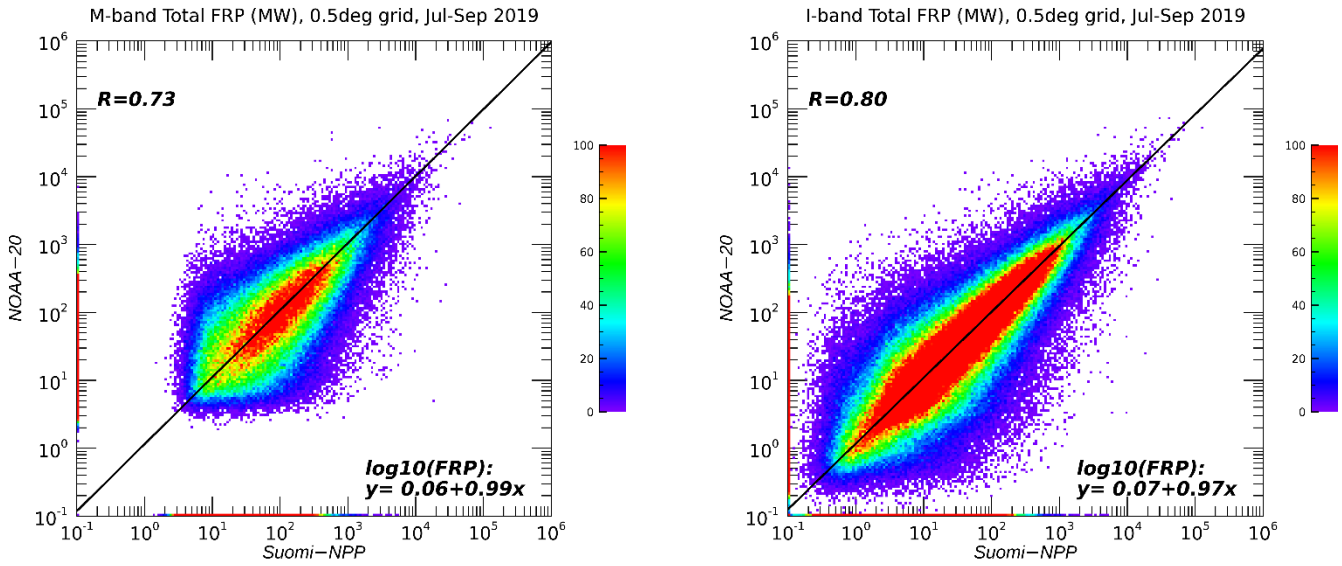

Figure 2-9: Frequency for M-band (left) and I-band (right) total fire radiative power (FRP) in 0.5x0.5 degree grid cell; global analysis for July-September, 2019.

2.5.7. Exception Handling

The software checks for bad, missing pixels (denoted by a fill value) and missing input data. It does not perform a retrieval in such cases.

2.6. Validation

2.6.1 *Validation Approach*

The validation approach adopted for the VIIRS active fire data builds on the heritage EOS/MODIS methodology, which consisted on the use of coincident reference fire data derived from higher spatial resolution sensors [Morisette *et al*., 2005; Schroeder *et al*., 2008]. However, the early afternoon orbit described by VIIRS is a major impediment limiting the use of available Landsat-class sensors (typically on ≈10am orbits) due to prohibitively large temporal separation between same-day data acquisitions [Csiszar and Schroeder, 2008]. As an alternative, reference data sets derived from airborne mapping instruments are used, complemented by field campaigns and other qualitative information originated from fire activity reports. Additionally, expert image analysts provide valuable input for the calculation of commission error rates associated with the occurrence of fire detection pixels in urban areas using available high-resolution visible imagery (e.g., Google Earth).

2.6.2 Validation Results

Data verification and validation was performed for selected sites across the globe, including dedicated field campaigns exploring small-to-medium size (<500 ha) prescribed fires (see for example: Dickinson *et al*. [2015]). Use of near-coincident airborne reference fire data shows good overall correspondence with VIIRS daytime and nighttime fire data generated for medium-to-large size wildfires as depicted in Figure 2-7.

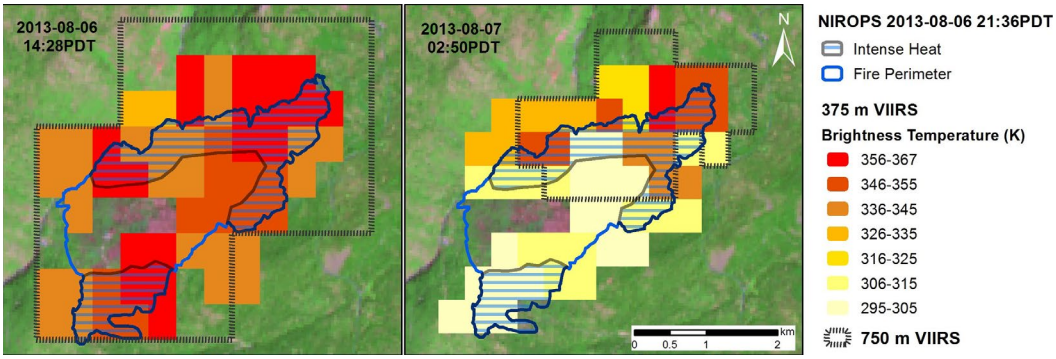

Figure 2-10: Airborne reference fire data (USDA/National Infrared Operations [NIROPs]) overlaid on near-coincident VIIRS daytime (left) and nighttime (right) 375 m fire detection data acquired on 06 and 07 August 2013, respectively. Outline of VIIRS 750 m baseline fire detection product is shown for reference (adapted from Schroeder *et al*. [2014]).

The occurrence of fire detection over urban areas (potential commission errors) was assessed by Schroeder *et al*. [2014] and was lower than 1.2% for nominal/high confidence pixels for all sites analyzed. Low confidence pixels responded for approximately 10% of all global fire pixels produced and showed higher occurrence of urban detections, peaking at 40% over eastern China where numerous industrial parks are found.

Comparison analyses of FRP retrievals derived using the approach above and those obtained from the VIIRS 750 m fire product (after reconciliation of the two data sets) shows good agreement (R^2=0.99) albeit with slightly (≈1%) lower values calculated for the latter. This difference is attributed to improved sampling of the background, which often results in cleaner data and higher FRP estimates. Given the spectral resolution of the M13 channel, in particular concerning the partial overlap with a CO_2 absorption band in the 4 μm region, atmospheric attenuation effects may double compared, for example, to the corresponding MODIS mid-infrared data (channels 21/22) used in the MOD14/MYD14 products (Figure 2-8). While this characteristic could lead to systematic underestimation of VIIRS FRP values compared to coincident MODIS data, other factors such as pixel size/geometry, data

aggregation and point spread function combine to create variable effects on FRP retrievals and the resulting correlation among products (Figure 2-9). Detailed assessment of FRP retrievals is currently limited to field validation campaigns that are few and sparse. Data verification and validation analyses shall expand as new reference data become available.

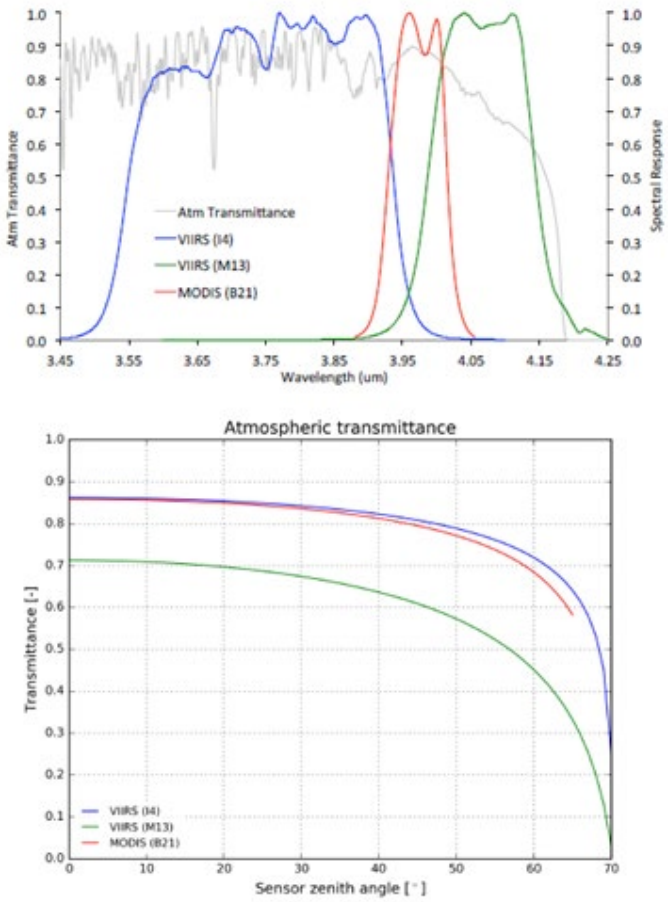

Figure 2-11: Spectral response functions for VIIRS I4 and M13, and MODIS B21/22 mid-infrared channels, and the corresponding atmospheric transmittance calculated using MODTRAN assuming U.S. standard atmospheric conditions (top panel). Bottom panel shows the corresponding net atmospheric transmittance as a function of the applicable VIIRS and MODIS sensor zenith angles.

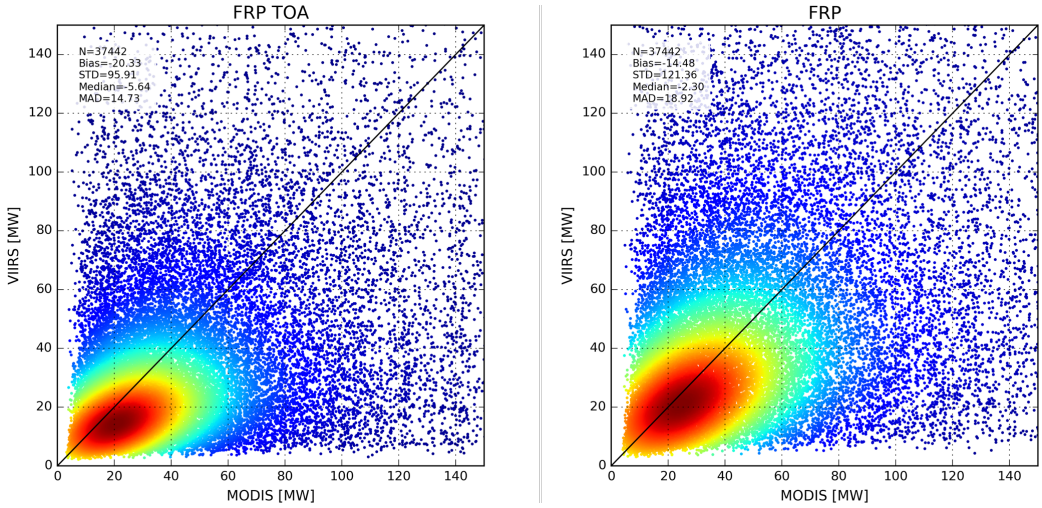

Figure 2-12: VIIRS M13 radiance-based FRP retrievals plotted against near-coincident Aqua/MODIS FRP (MYD14). Left panel shows top-of-atmosphere (TOA) data; right panel shows same data after atmospheric correction using MODTRAN® and MERRA 0.5º global analysis data.

3. ASSUMPTIONS AND LIMITATIONS

3.1. Performance Assumptions

Algorithm performance is dependent on observation conditions and therefore will be degraded when optically thick clouds and/or heavy smoke plumes are in the line of sight. Also, stronger attenuation of the M13 channel radiance is expected, leading to subsequent underestimation of FRP. Additionally, the pixel's point spread function (PSF) can and will affect product performance, reducing the sensor response to sub-pixel fires and the corresponding probability of detection along with increase in FRP retrieval errors [Schroeder *et al.*, 2010].

3.2. Potential Improvements

Work is ongoing to improve the I-band algorithm performance. Several caveats are identified as result of the product analysis identifying areas of potential improvement:

- FRP calculation depends on background window pixels' availability, if there are not enough background pixels in a search window the fire is detected but FRP is set to zero. While in general it is infrequent situation, it was found important for large fires where big clusters of fire pixels are detected in search window, and background radiance cannot be retrieved. Threshold relaxation for spatial heterogeneity test is expected to improve per fire FRP estimates.

- Large fires produce significant amount of smoke, and sometimes smoke is hot enough to be identified as a fire in the algorithm. Reducing false alarms from hot smoke plumes will improve the algorithm performance.
- FRP is retrieved from TOA radiances, different scan angles may impact the FRP calculation. Applying atmospheric correction is expected to improve FRP retrieval.
- NOAA-20 bad I3 detector results in some fire detections being lost; the algorithm fix is going to be implemented.

4. REFERENCES

Cabrera, J., Cyamukungu, M., Stauning, P., Leonov, A., Leleux, P., Lemaire, J., *et al*. (2005). Fluxes of energetic protons and electrons measured on board the Oersted satellite. *Annales Geophysicae*, 23, 2,975-2,982.

Cao, C., De Luccia, F.J., Xiong, X., Wolfe, R., Weng, F. (2014). Early on-orbit performance of the Visible Infrared Imaging Radiometer Suite onboard the Suomi National Polar-Orbiting Partnership (S-NPP) satellite. *IEEE Transactions on Geoscience and Remote Sensing*, 52, 1142-1156.

Casadio, S., Arino, O., and Serpe, D. (2012). Gas flaring monitoring from space using ATSR instrument series. *Remote Sensing of Environment*, 116, 239-249.

Csiszar, I., Morisette, J., Giglio, L. (2006). Validation of active fire detection from moderate resolution satellite sensors: the MODIS example in Northern Eurasia. *IEEE Transactions on Geoscience and Remote Sensing*, vol. 44, no. 7, 1757-1764.

Csiszar, I. and W. Schroeder (2008). Short-Term Observations of the Temporal Development of Active Fires from Consecutive Same-Day ETM+ and ASTER Imagery in the Amazon: Implications for Active Fire Product Validation. *IEEE Journal of Selected Topics in Earth Observations and Remote Sensing*, Vol. 1, No. 4, 248-253. DOI: 10.1109/JSTARS.2008.2011377.

Csiszar, I., Schroeder, W., Giglio, L., Ellicott, E., Vadrevu, K. P., Justice, C. O., Wind, B. (2014). Active fires from the Suomi NPP Visible Infrared Imaging Radiometer Suite: Product status and first evaluation results, *J Geophys Res Atmos*, 119, doi:10.1002/2013JD020453.

Dickinson, M.B., Hudak, A.T., Zajkowski, T., Loudermilk, L.E., Schroeder W., *et al*. (2015). Measuring radiant emissions from entire prescribed fires with ground, airborne and satellite sensors – RxCADRE 2012. *International Journal of Wildland Fire*, doi: 10.1071/WF15090.

Giglio, L., Descloitres, J., Justice, C. O., Kaufman, Y. J. (2003). An enhanced contextual fire detection algorithm for MODIS. *Remote Sensing of Environment*, 87, 273–282.

Giglio, L., Schroeder, W., Justice, C.O. (2016). The Collection 6 MODIS Active Fire Detection Algorithm and Fire Products. *Remote Sensing of Environment,* 178 31-41 doi:10.1016/j.rse.2016.02.054.

Global Volcanism Program, 2013. Volcanoes of the World, v. 4.8.5. Venzke, E (ed.). Smithsonian Institution. Downloaded 13 Nov 2019. https://doi.org/10.5479/si.GVP.VOTW4-2013

Kaufman, Y.J., Justice, C.O., Flynn, L.P., Kendall, J.D., Prins, E.M., Giglio, L., et al. (1998). Potential global fire monitoring from EOS-MODIS. *Journal of Geophysical Research*, 103 (D24), 32,215-32,238.

Liu, Yongxue & Hu, Chuanmin & Zhan, Wenfeng & Sun, Chao & Murch, Brock & Ma, Lei. (2017). Identifying industrial heat sources using time-series of the VIIRS Nightfire product with an object-oriented approach. Remote Sensing of Environment. 204. 10.1016/j.rse.2017.10.019.

Lobert, J.M., and Warnatz, J. (1993). Emissions from the combustion process in vegetation. In P.J. Crutzen and J.G. Goldammer (Eds.), *Fire in the environment: The ecological, atmospheric, and climatic importance of vegetation fires* (pp. 15-37). John Wiley & Sons Ltd.Morisette, J.T., Giglio, L., Csiszar, I. , Justice, C.O. (2005a). Validation of the MODIS active fire product over Southern Africa with ASTER data. *International Journal of Remote Sensing*, 26:4239–4264.

Morisette, J.T., Giglio, L., Csiszar, I., Setzer, A., Schroeder, W., Morton, D., Justice, C.O. (2005b). Validation of MODIS active fire detection products derived from two algorithms. *Earth Interactions*, 9:1-23.

Schroeder, W., Prins, E., Giglio, L., Csiszar, I., Schimdt, C., Morisette, J., Morton, D. (2008a). Validation of GOES and MODIS active fire detection products using ASTER and ETM+ data. *Remote Sensing of Environment*, 112 (2008) 2711–2726.

Schroeder, W., Ruminski, M., Csiszar, I., Giglio, L., Prins, E., Schmidt, C., Morisette, J. (2008b): Validation Analyses of and Operational Fire Monitoring Product: the Hazard Mapping System. *International Journal of Remote Sensing*, Vol. 29, No. 20, 6059–6066, DOI: 10.1080/01431160802235845.

Schroeder, W., Csiszar, I., Giglio, L., and Schmidt, C.C. (2010). On the use of fire radiative power, area, and temperature estimates to characterize biomass burning via moderate to coarse spatial resolution remote sensing data in the Brazilian Amazon. *Journal of Geophysical Research*, 115, doi:10.1029/2009JD013769.

Schueler, C.F., Lee, T.F., and Miller, S.D. (2013). VIIRS constant spatial resolution advantages. *International Journal of Remote Sensing*, 34, 5761-5777.

Schroeder, W., Oliva, P., Giglio, L., and Csiszar, I. (2014). The new VIIRS 375 m active fire detection data product: Algorithm description and initial assessment. *Remote Sensing of Environment*, 143, 85-96.

Wolfe, R.E., Lin, G., Nishihama, M., Tewari, K.P., Tilton, J.C., and Isaacman, A.R. (2013). Suomi NPP VIIRS prelaunch and on-orbit geometric calibration and characterization. *Journal of Geophysical Research: Atmospheres*, 118, doi:10.1002/jgrd.50873.

Wooster, M. J., Zhukov, B., and Oertel, D. (2003). Fire radiative energy for quantitative study of biomass burning: derivation from the BIRD experimental satellite and comparison to MODIS fire products. *Remote Sensing of Environment,* 86, 83–107.

END OF DOCUMENT